

Received January 7, 2020, accepted February 3, 2020, date of publication February 7, 2020, date of current version February 17, 2020.

Digital Object Identifier 10.1109/ACCESS.2020.2972504

Image Correlation Using Fractional Hermite Transform

ALFREDO CASTRO-VALDEZ¹ AND JOSUÉ ÁLVAREZ-BORREGO¹

Applied Physics Division, Optics Department, CICESE, Ensenada 22860, Mexico

Corresponding author: Josué Álvarez-Borrego (josue@cicese.mx)

This work was supported by the Centro de Investigación Científica y de Educación Superior de Ensenada, B. C. (CICESE).

ABSTRACT In this paper, we generalize the Hermite transform into a fractional case using the fractional Fourier transform and the fractional convolution. The new methodology was evaluated using phytoplankton images with different illumination patterns and fragmented images. We found that the fractional Hermite transform had a better capability to recognize images. The discrimination coefficient was evaluated for the fractional Hermite transform and the conventional Hermite transform, finding more noise tolerate with the fractional Hermite transform. The Hermite fractional transform, in combination with the extreme phase filter, showed in a study, using fragmented diatom images, a better ability to classify diatoms, even when these had little information.

INDEX TERMS Fractional convolution, fractional Hermite transform, pattern recognition, Pearson correlation.

I. INTRODUCTION

Over 50 years ago, Vander Lugt began a change in the way of using the Fourier transform in optics by introducing a methodology for filtering space and signal detection [1]. Recently the area of optics has been extended by using new variations in transforms. Transforms that before were only defined for whole cases have been generalized to fractional cases. Such as the fractional Fourier transform [2]–[5], the fractional Hilbert transform [6], [7], the Hankel transform, [8], and the Hartley transform [9]. The fact of having generalized the transforms have allowed finding better results; the fractional Hilbert transform can be applied to the detection of edges [10]–[13]. However, the most used fractional transform has been the Fourier transform. It has applications in different fields, such as Fourier optics [14], [15], convolution [16], image restoration [17], correlation [18]–[20], non-linear optics [21], quantum mechanics [22] and, filtering [23], recognition of objects [24], [25]. Another particularity of the fractional Fourier transform is that from it, we can define other fractional transforms, such as the fractional Hilbert transform [6]. The correlation between the two functions is more straightforward using the Fourier transform and the frequential plane [26]. This property was extended to the fractional Fourier transform, defining the fractional correlation and the fractional convolution [3], [18]. Another transform used is the Hermite transform, which is a particular case of the

polynomial transforms [27]. The Hermite transform appears when the polynomials used in the transform are Hermite polynomials [28]. This transform has applications in different fields, has been used for iris recognition [29], estimation in cardiac CT [30], and fetal echocardiography [31]. It has been applied to noise reduction and image fusion [32], [33], to make neural network correlation using simulated radar signals [34]. In this article, we generalized the Hermite transform into the fractional Hermite transform, and with this increase, the ability to recognize patterns.

II. 2-D HERMITE TRANSFORM

The Hermite transform is a particular case of polynomial transforms; it can be considered as an image description model. This transform is a technique of signal decomposition. The analysis has two steps. First, an input signal $L(x, y)$ is multiplied by a window function,

$$v(x - p, y - q), \quad (1)$$

at the positions p and q .

The objective is achieving a complete description of the signal; this process is repeated in several positions equidistant from the window on the image, forming with these positions a sampling grid S , where for each (x, y) the pixel coordinates and the input signal is multiplied by the window function, and the original signal is

$$L(x, y) = \frac{1}{W(x, y)} \sum_{p, q \in S} L(x, y) v(x - p, y - q), \quad (2)$$

The associate editor coordinating the review of this manuscript and approving it for publication was Byung-Gyu Kim¹.

where,

$$W(x, y) = \sum_{p, q \in S} v(x - p, y - q), \quad (3)$$

is a weighting function.

The only condition is that eq. (3) will be different from zero in all (x, y) .

Second, the signal in the window is described using a weighting sum of $G_{m,n-m}(x, y)$ with grades m and, $n - m$ respect to x, y .

The polynomials are defined by a window function,

$$\int_{-\infty}^{\infty} \int_{-\infty}^{\infty} v^2(x, y) G_{m,n-m}(x, y) \times G_{l,k-l}(x, y) dx dy = \delta_{nl} \delta_{mk}, \quad (4)$$

where, $n, l = 0, 1, 2, \dots, \infty$; $m, k = 0, 1, 2, \dots, \infty$, δ_{nl}, δ_{mk} are the Kronecker function and, \times is a point-by-point multiplication.

The process of mapping the input signal into a weighted sum of polynomials, called polynomial coefficients, is known as a direct polynomial transform.

The polynomial coefficients $L_{m,n-m}(p, q)$ are calculated by convolving the original image with the analysis filters

$$D_{m,n-m}(x, y) = G_{m,n-m}(x, y) v^2(-x, -y) \quad (5)$$

that is, for everything, $(p, q) \in S$,

$$L_{m,n-m}(p, q) = \int_{-\infty}^{\infty} \int_{-\infty}^{\infty} L(x, y) \times D_{m,n-m}(x - p, y - q) dx dy. \quad (6)$$

where,

$$G_{m,n-m}(x, y) = \frac{1}{\sqrt{2^n(n-m)!m!}} \times H_m\left(\frac{x}{\sigma}\right) H_{n-m}\left(\frac{y}{\sigma}\right), \quad (7)$$

$$v(x, y) = \frac{1}{\sqrt{\sqrt{\pi}\sigma}} e^{-\frac{x^2+y^2}{2\sigma^2}}, \quad (8)$$

where $v(x, y)$ is a Gaussian window function, σ is the standard deviation of the Gaussian window function and,

$$H_n(x) = (-1)^n e^{x^2} \frac{d^n}{dx^n} e^{-x^2}, \quad n = 0, 1, 2, \dots \quad (9)$$

where $H_n(x)$ is the n -th Hermite polynomial.

Using the convolution form in eq. (6) it is defined as,

$$L_{m,n-m}(p, q) = L(x, y) * D_{m,n-m}(x, y) \quad (10)$$

III. CONVOLUTION

Convolution between two functions $f(x, y)$ and $g(x, y)$, is defined as,

$$h(x, y) = \int_{-\infty}^{\infty} \int_{-\infty}^{\infty} f(\xi, \eta) g(x - \xi, y - \eta) d\xi d\eta, \quad (11)$$

where ξ, η are the integration variables which do the displacements.

The convolution property [35] of the conventional Fourier transform is given as,

$$\mathbb{F}\{f(x, y) * g(x, y)\} = F(u, v)G(u, v), \quad (12)$$

where, \mathbb{F} is the Fourier transform operator, (x, y) are the space variables and, (u, v) are the frequency variables.

It is possible to find the convolution between two functions by the Fourier transform,

$$f(x, y) * g(x, y) = \mathbb{F}^{-1}\{F(u, v)G(u, v)\}, \quad (13)$$

and, in eq. (10), using $L(x, y) = f(x, y)$ and, $D_{m,n-m}(x, y) = g(x, y)$, it can be express as,

$$L_{m,n-m}(p, q) = \mathbb{F}^{-1}\left\{\frac{\mathbb{F}\{L(x, y)\} \times \mathbb{F}\{D_{m,n-m}(x, y)\}}{\mathbb{F}\{D_{m,n-m}(x, y)\}}\right\}. \quad (14)$$

Now, the Hermite transform will be express as a convolution between an input image $L(x, y)$ and, the analysis filters $D_{m,n-m}(x, y)$, using the Fourier transform.

IV. FRACTIONAL CONVOLUTION

An advantage of using Fourier formalism is that there is the fractional Fourier transform [5], defined as follows,

$$F^\alpha(u) = \mathbb{F}^\alpha\{f(x)\} = \sqrt{1 - \cot \phi} \times e^{i\pi u^2 \cot \phi} \int_{-\infty}^{\infty} f(x) e^{i\pi x^2 \cot \phi} e^{-2i\pi ux \csc \phi} dx, \quad (15)$$

The Eq.(15) is defined as the α order of the fractional Fourier transform, with,

$$\phi = \frac{\alpha\pi}{2}. \quad (16)$$

In this way, a fractional convolution can be generated using the fractional Fourier transform [36]. Using (13) as follows,

$$f(x, y) *_{\alpha} g(x, y) = \mathbb{F}^{-\alpha}\left\{\frac{\mathbb{F}^\alpha\{f(x, y)\} \times \mathbb{F}^\alpha\{g(x, y)\}}{\mathbb{F}^\alpha\{g(x, y)\}}\right\}. \quad (17)$$

As eq. (14), which represents the Hermite transform as a convolution, now using the fractional convolution the fractional Hermite transform acquires an additional factor α given by the fractional convolution which modifies its behavior, this fractional transform is represented as,

$$L_{m,n-m,\alpha}(p, q) = \mathbb{F}^{-\alpha}\left\{\frac{\mathbb{F}^\alpha\{L(x, y)\} \times \mathbb{F}^\alpha\{D_{m,n-m}(x, y)\}}{\mathbb{F}^\alpha\{D_{m,n-m}(x, y)\}}\right\}. \quad (18)$$

For the same values of m and n by varying the value of α the convolution can be changed. The α value can be varied from 0 to 1, where $\alpha = 0$ it is equivalent to multiplying the input image by the filter associated with the order of the Hermite transform and $\alpha = 1$ is the Hermite transform of order m and n . For values between 0 and one, the Fractional Transform of Hermite is obtained (Fig. 1).

The Hermite transform has been used to highlight edges, this new parameter modifies the edges, and it could increase the capability of image recognition. Different metrics were used to test this additional factor, in which the α value was adaptive to find the optimal order.

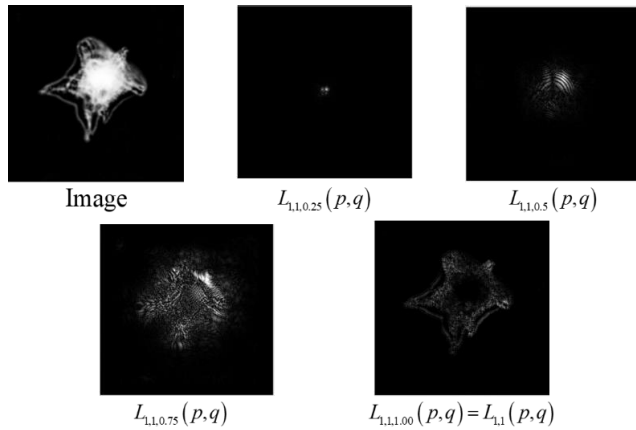


FIGURE 1. Different orders to the fractional Fourier transform, using the order $L_{1,1}$ in Hermite transform.

V. METRICS

Different metrics quantify the ability of a methodology to recognize an objective image. Among these metrics is the Discrimination Coefficient (DC) and the peak-to-Correlation Energy (PCE).

The discrimination coefficient evaluates the filtering skill to detect an object immersed in noise. This coefficient is given by [37],

$$DC = 1 - \frac{|C_{I-R}|^2}{|C_{I-IR}|^2}, \tag{19}$$

where C_{I-R} is the maximum value of the correlation plane between the target image and the background image (noise) and C_{I-IR} is the maximum value of the correlation plane between the target image and the target image affected by noise. The maximum value of this metric is one when the target image does not present noise. When the discrimination coefficient value is zero or negative, it indicates a target image very immersed in noise. Therefore, the filter cannot recognize the target image.

The PCE value is a relation of the energy at the origin, which compares the total energy of the correlation plane with the value of the correlation peak energy,

$$PCE = \frac{|E\{C(0,0)\}|^2}{E\{|C(x,y)|^2\}}, \tag{20}$$

where the numerator is the square module of the expected value of the intensity of the correlation peak and, $C(0,0)$ is the correlation plane center, in which the correlation value has its maximum value.

The denominator is the square module of the expected value of the average energy in the correlation plane at pixels (x,y) [38].

The noise added to the images were Gaussian and impulsive, to visualize these noises were applied in letter E (Fig. 2).

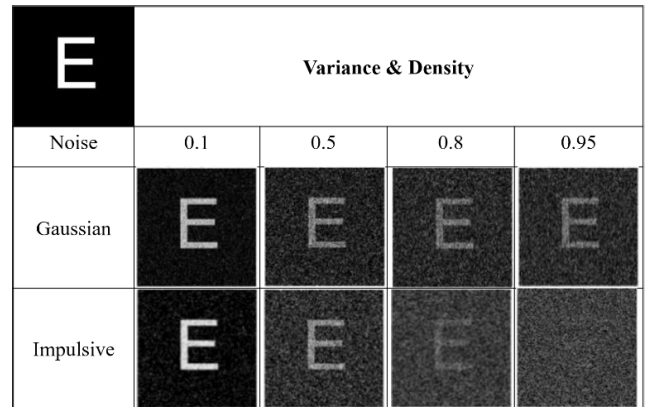


FIGURE 2. The image of the letter E is shown with different values of variance and density for the Gaussian and impulsive noises respectively.

VI. METHODOLOGY

Comparisons were made between three methodologies to know the capacity of each one. The first case consisted of doing the conventional correlation, which takes the input images, then applied the Fourier transform to the images, do the point-by-point multiplication, applied the inverse Fourier transform to the result and, finally obtain the correlation plane. The second case was using the Hermite transform $L_{1,1}$ with which better correlation values are obtained [39], in this case, the input images are modified using the Hermite transform before applying the Fourier transform and do the correlation. In the third case, the fractional Hermite transform with the optimal order was used for each image before the Fourier transform.

To find the optimal fractional order of the Hermite transform $L_{1,1}$ the values $.61 \leq \alpha \leq 1.0$ in (18) were applied. For each value of α , an auto-correlation was performed, and the correlation value was calculated. Use $\alpha \geq 0.61$ ensures a correlation more representative than use small α values in which not enough information is obtained. The optimal order selected corresponds to the maximum correlation value for each target.

VII. RESULTS

The discrimination coefficient for Gaussian and impulsive noises were calculated comparing the Hermite transform to the Hermite fractional transform (order $\alpha = 0.61$). Also, it was obtained the discrimination coefficient for the image with classical correlation.

With the Gaussian noise, using a noise variance up to 5, the three methodologies were capable of recognizing the input image. The classic filter was used to probe the discrimination coefficient; this produced a better noise tolerance in the conventional correlation, which has a DC of 0.98 with a variance of 5. Using the same parameters with the Hermite transform $L_{1,1}$, and the fractional Hermite transform $L_{1,1}$, the DC values obtained were 0.75 and 0.88, respectively.

With the impulsive noise, the three methodologies showed an acceptable tolerance. The DC value was close to one to

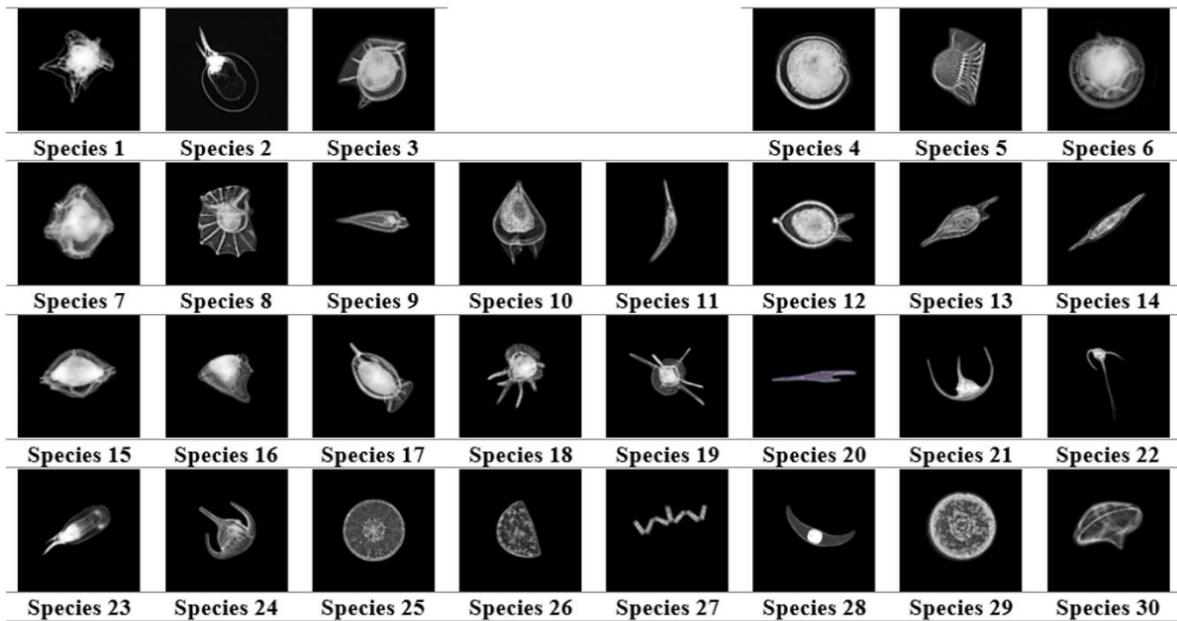


FIGURE 3. Phytoplankton species. Species 1 is *Acanthogonyaulax spinifera*. Species 2 is *Ceratium gravidum*. Species 3 is *Dinophysis hastata*. Species 4 is *Diplosalopsis orbicularis*. Species 5 is *Histioneis*. Species 6 is *Lingulodinium polyedrum*. Species 7 is *Ornithocercu armata*. Species 8 is *Ornithocercus magnificus*. Species 9 is *Oxytoxum scolapax*. Species 10 is *Podolampas bipes 1*. Species 11 is *Podolampas spinifer 1*. Species 12 is *Podolampas bipes 2*. Species 13 is *Podolampas palmipes*. Species 14 is *Podolampas spinifer 2*. Species 15 is *Protoperidinium*. Species 16 is *Dinophysis rapa*. Species 17 is *Dinophysis hastate*. Species 18 is *Ceratocorys horrida 1*. Species 19 is *Ceratocorys horrida 2*. Species 20 is *Ceratium furca*. Species 21 is *Ceratium lunula*. Species 22 is *Ceratium hexacantum*. Species 23 is *Ceratium praelongum*. Species 24 is *Ceratium breve*. Species 25 is *Asterolampra marylandica*. Species 26 is *Hemidiscus cuneiformis*. Species 27 is *Thalassionema nitzschioides*. Species 28 is *Pyrocystis*. Species 29 is *Hemidiscus*. Species 30 is *Dinoflagellata*.

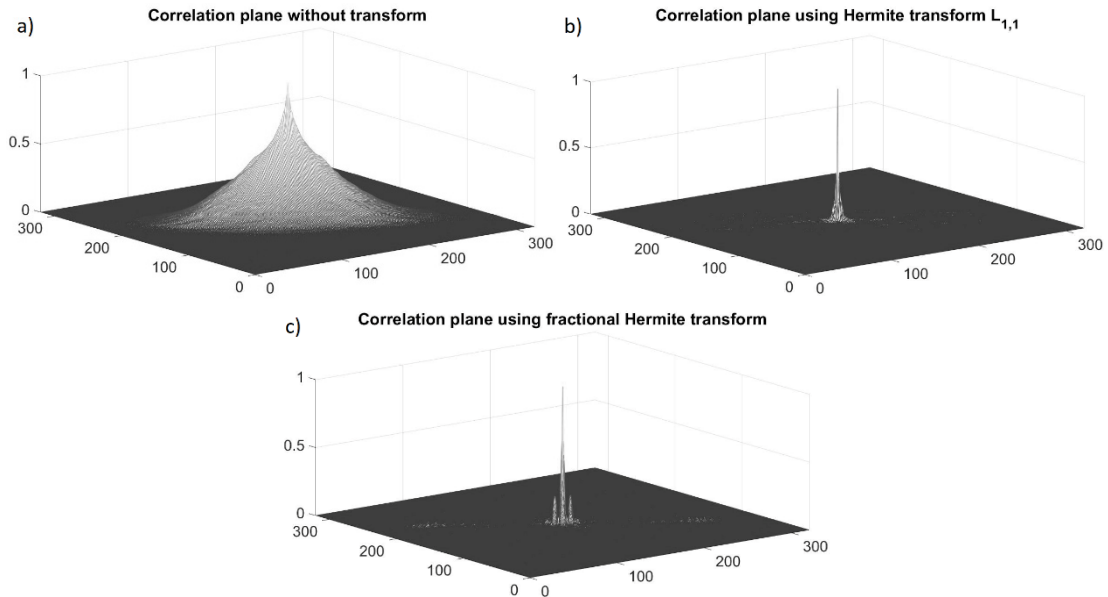


FIGURE 4. Correlation plane using three different methodologies. Using a) Classic correlation. b) Hermite correlation. c) Fractional Hermite correlation $\alpha = 0.75$.

a noise density of 90% using the conventional correlation, in the case of using Hermite transform $L_{1,1}$, the DC remained close to one until a noise density of 75% and the fractional Hermite transform until 80%.

The conventional case showed higher tolerance to Gaussian and impulsive noise, due that the classic filter was used and had a better noise tolerance. However, a comparison between the Hermite transform and the fractional Hermite

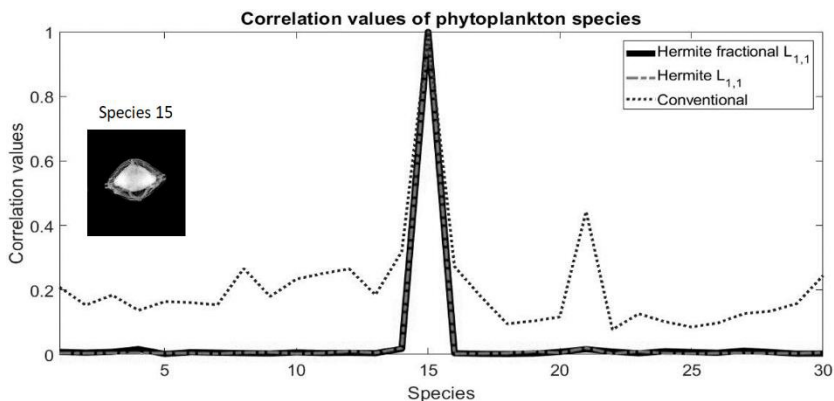


FIGURE 5. Correlation values between 30 phytoplankton species using species 15 as a filter.

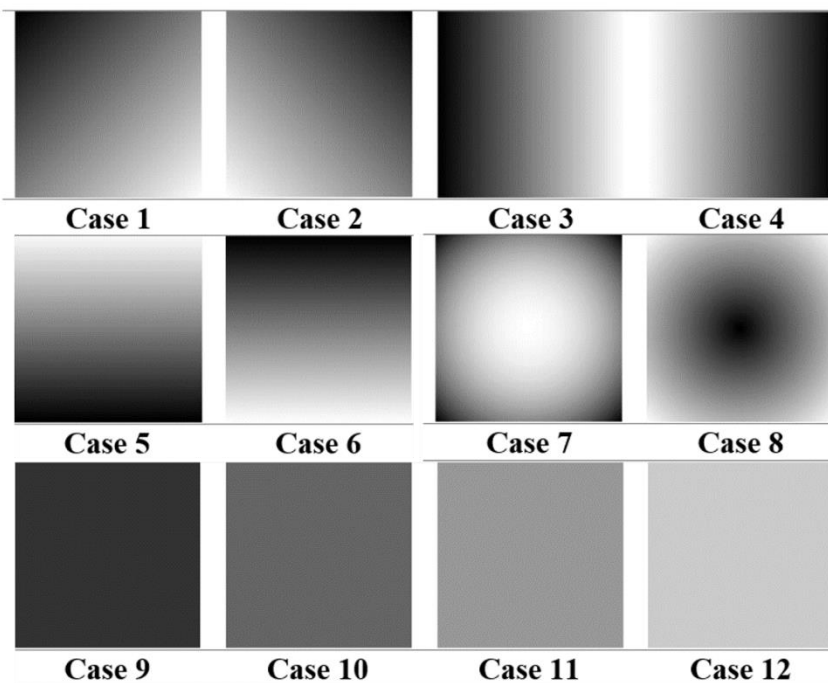


FIGURE 6. Illumination patterns used in the phytoplankton species images.

transform showed a better noise tolerance to the fractional one.

To probe the methodologies images of phytoplankton species with the black background of 320×320 pixel size were used, these are shown in Fig. 3.

For each species, the optimal order of the fractional Hermite transform was calculated using the maximum correlation value as a parameter; the optimal values are shown in Table 1.

Correlations were made with a classic filter and, with the correlation values obtained, the three methodologies were compared.

Using a classic filter, species 1 was auto-correlated in the conventional form, also using the Hermite transform $L_{1,1}$ and, the fractional Hermite transform with $\alpha = 0.75$. The correlation plane showed the correlation value and the PCE for each case; the conventional correlation produces a lower

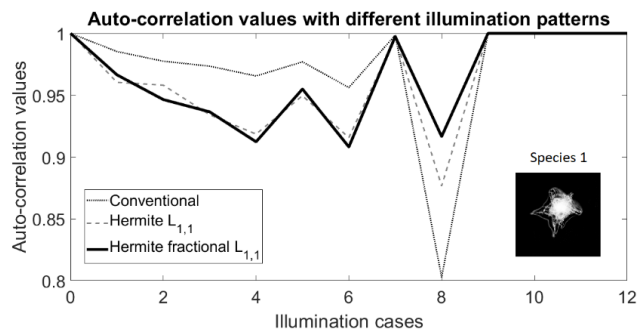


FIGURE 7. Correlation values of species 1 with different illumination patterns.

PCE (Fig. 4a), which indicates a weak capacity of recognition in comparison with the Hermite transform, which produces a better PCE (Fig. 4b), therefore a higher ability to identify

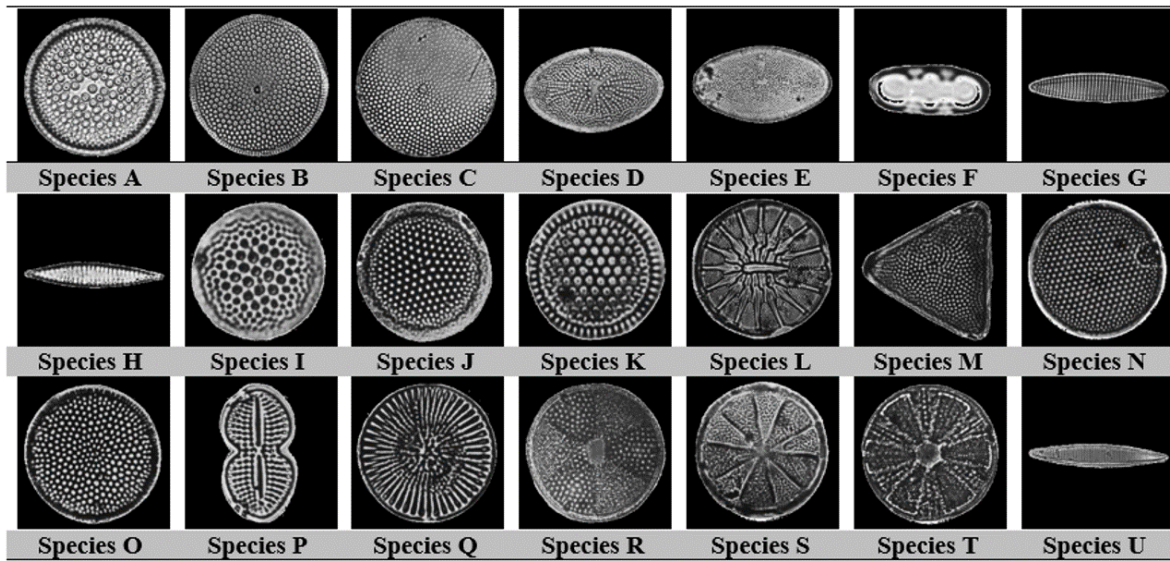


FIGURE 8. Fossilized diatoms, Species A: *Actinocyclus ingens*. Species B: *Azpeltia* sp. Species C: *Azpeltia nodulifera*. Species D: *Actinocyclus ellipticus* var. *Moronensis*. Species E: *Denticulopsis pradimorpha*. Species G: *Nitzschia praereinholdii*. Species H: *Bogorovia praepaleacea*. Species I: *Thalassiosira oestrupii* var 1. Species J: *Thalassiosira oestrupii* var 2. Species K: *Thalassiosira domifacta*. Species L: *Asteromphalus imbricatus*. Species M: *Pseudotriceratium cinnamomeum*. Species N: *Thalassiosira kozlovii*. Species O: *Coscinodiscus radiatus*. Species P: *Diploneis bombus*. Species Q: *Stephanodiscus* sp. Species R: *Actinoptychus undulatus*. Species S: *Actinoptychus bipunctatus*. Species T: *Actinoptychus splendens*. Species U: *Nitzschia reinholdii*.

TABLE 1. Optimal order to each species using the fractional Hermite transform.

Species	Optimal order (α)	Species	Optimal order (α)	Species	Optimal order (α)	Species	Optimal order (α)	Species	Optimal order (α)
1	0.75	7	0.82	13	0.75	19	0.86	25	0.79
2	0.82	8	0.84	14	0.78	20	0.70	26	0.73
3	0.68	9	0.87	15	0.77	21	0.66	27	0.75
4	0.71	10	0.72	16	0.86	22	0.65	28	0.78
5	0.94	11	0.80	17	0.89	23	0.81	29	0.85
6	0.77	12	0.81	18	0.87	24	0.75	30	0.95

TABLE 2. Optimal order of fractional Hermite transform for each diatom species.

Species A	0.74	Species H	0.79	Species O	0.74
Species B	0.76	Species I	0.79	Species P	0.72
Species C	0.77	Species J	0.77	Species Q	0.75
Species D	0.83	Species K	0.79	Species R	0.73
Species E	0.61	Species L	0.67	Species S	0.77
Species F	0.62	Species M	0.74	Species T	0.70
Species G	0.73	Species N	0.77	Species U	0.76

the input image. This behavior is the same as the fractional Hermite transform, which has a high PCE value (Fig. 4c).

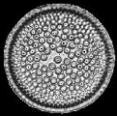
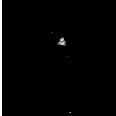


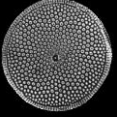
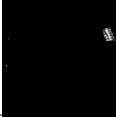
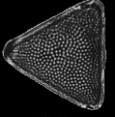

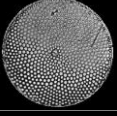
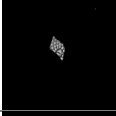
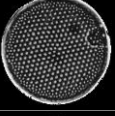


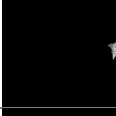
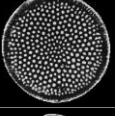


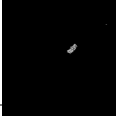




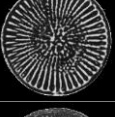



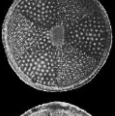





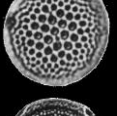
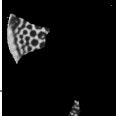


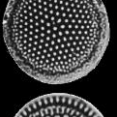

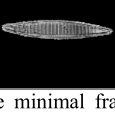
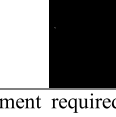


For the 30 species, the correlation value was plotted to find that the fractional Hermite transform produces excellent results in comparison with those obtained with the conventional correlation. We can distinguish every species using the three methods. However, the cross-correlation results obtained with Hermite and fractional Hermite transform are smaller than using conventional correlation; these smaller correlation values produce a higher reliability level (Fig. 5).

Applying 12 different illumination patterns were contemplated to evaluate the recognition capability of the methodologies (Fig. 6).

It was found that the fractional methodology is more tolerant in the worst illumination. In the illumination pattern 8, it can be seen that the fractional Hermite transform has a higher correlation value than the other methodologies (Fig. 7).

Table 1 shows the different optimal order for each species, every order highlight component of each species since every species has an optimal order, this order helps to highlight

TABLE 3. Minimum information required to identify each diatom species.

Species	Filter	MRF	MPRC	MPRH	MPR	Species	Filter	MRF	MPRC	MPRH	MPR
A			1.08%	1.08%	0.46%	L			1.93%	1.93%	0.70%
B			2.97%	2.97%	1.12%	M			5.96%	5.96%	1.71%
C			2.05%	2.05%	2.05%	N			18.7%	18.7%	5.74%
D			5.92%	5.92%	1.51%	O			1.98%	1.98%	0.66%
E			4.2%	4.2%	0.94%	P			7.9%	7.9%	2.47%
F			10.8%	10.8%	10.8%	Q			8.21%	8.21%	0.59%
G			7.29%	7.29%	7.29%	R			7.19%	7.19%	0.80%
H			4.61%	4.61%	3.70%	S			10.96%	10.96%	0.73%
I			21.48%	21.48%	13.39%	T			4.9%	4.9%	1.14%
J			4.96%	4.96%	3.98%	U			4.05%	4.05%	1.82%
K			25.36%	25.36%	15.03%	*MRF is the minimal fragment required using the fractional Hermite transform. MPRC is the minimal percent required with conventional correlation. MPRH is the minimal percent required with Hermite transform. MPR is the minimal percent corresponding to MRF.					

the components of his species and identify the species with higher confidence.

Twenty-one species of fossilized diatoms (Fig. 8) with 50 fragmented variants per species were used (Fig. 9).

For each diatom species, the optimal order of fractional Hermite transform was calculated, these orders increase the capability of species identification even with fragmented images (Table 2).

Correlations were made with the three methodologies. For each species, the correlation value from the complete sample to the 50th sample was selected, and it was verified that the maximum cross-correlation value was not higher than the minimum correlation value between the same species. This limit corresponds to the ability to distinguish the target species when it is fragmented. The values of this capacity are shown in Table 3.

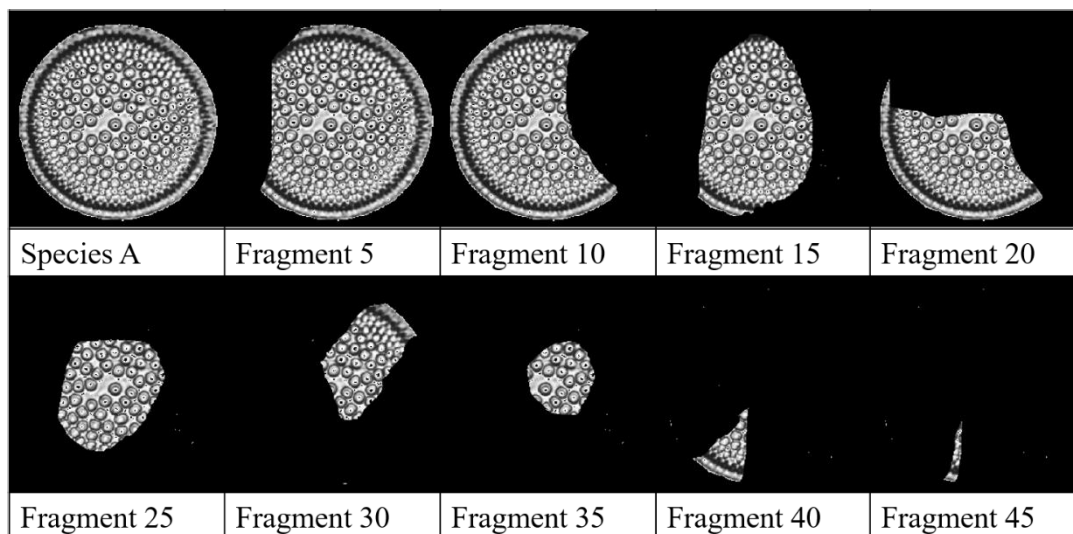


FIGURE 9. Some diatoms fragments used in correlations.

The fragment number required to identify each species is minimal using the extreme phase filter and fractional Hermite transform results shown in Table 3. Since the fractional Hermite transform highlights the edges and has a higher noise tolerance compare with Hermite transform, its ability to recognized fragmented diatoms is better.

Table 3 shows a higher capacity to recognized fragmented diatoms even with a little information comparing with other methodologies; this raises the confidence level of diatoms classification.

The Hermite transform highlights the edges in the image that was applied; now, the optimal α value also provides a specifically highlighted edges to each species; this increases the capability of recognizing species even with few fragments.

The results obtained by conventional correlation and using the Hermite transform are equals because the extreme phase filter produces similar correlation values in both correlations.

VIII. CONCLUSION

In this work were evaluated three correlation methodologies, one used a control methodology which only had the Fourier transform and two based on the Hermite transform and the fractional Hermite transform. The results show that exist different optimal orders to each image in which the fractional Hermite transform could support more noise intensity than the conventional Hermite transform and produces a higher PCE value than the conventional correlation. The fractional Hermite transform could identify all the phytoplankton species with a sufficient discrimination capacity, even when the images had different illumination patterns, shown a better identification capacity than the classical correlation and conventional Hermite transform. The fractional methodology responds better than the others when it was tested with fragmented diatoms. Using extreme phase filter

was possible to identify all the fragmented diatoms even with a little part of the information. The new fractional correlation presented has more noise tolerance and identification power than using conventional transforms.

REFERENCES

- [1] A. Lugt, "Signal detection by complex spatial filtering," *IEEE Trans. Inf. Theory*, vol. IT-10, no. 2, pp. 139–145, Apr. 1964.
- [2] D. Mendlovic and H. M. Ozaktas, "Fractional Fourier transforms and their optical implementation: I," *J. Opt. Soc. Amer. A, Opt. Image Sci.*, vol. 10, no. 9, p. 1875, Sep. 1993.
- [3] P. Pellat-Finiet, "Fresnel diffraction and the fractional-order Fourier transform," *Opt. Lett.*, vol. 19, no. 18, pp. 1388–1390, Sep. 1994.
- [4] H. M. Ozaktas and D. Mendlovic, "Fractional Fourier optics," *J. Opt. Soc. Amer. A, Opt. Image Sci.*, vol. 12, no. 4, pp. 743–751, 1995.
- [5] H. M. Ozaktas, M. A. Kutay, and D. Mendlovic, "Advances in imaging and electron physics," in *Introduction to the Fractional Fourier Transform and its Applications*. P. W. Hawkes, Ed. New York, NY, USA: Academic, 1999, ch. 4, pp. 239–291.
- [6] A. W. Lohmann, D. Mendlovic, and Z. Zalevsky, "Fractional Hilbert transform," *Opt. Lett.*, vol. 21, no. 4, pp. 281–283, 1996.
- [7] A. W. Lohmann, E. Tepichín, and J. G. Ramírez, "Optical implementation of the fractional Hilbert transform for two-dimensional objects," *Appl. Opt.*, vol. 36, no. 26, pp. 6620–6626, Sep. 1997.
- [8] H.-Y. Fan, "Fractional Hankel transform studied by charge-amplitude state representations and complex fractional Fourier transformation," *Opt. Lett.*, vol. 28, no. 22, pp. 2177–2179, Nov. 2003.
- [9] S.-C. Pei, C.-C. Tseng, M.-H. Yeh, and J.-J. Shyu, "Discrete fractional Hartley and Fourier transforms," *IEEE Trans. Circuits Syst. II. Analog Digit. Signal Process.*, vol. 45, no. 6, pp. 665–675, Jun. 1998.
- [10] J. A. Davis, D. E. McNamara, and D. M. Cottrell, "Analysis of the fractional Hilbert transform," *Appl. Opt.*, vol. 37, no. 29, pp. 6911–6913, Oct. 1998.
- [11] M.-H. Yeh and S.-C. Pei, "Discrete fractional Hilbert transform," *IEEE Trans. Circuits Syst. II, Exp. Briefs*, vol. 47, no. 11, pp. 1307–1311, Nov. 2000.
- [12] C.-C. Tseng and S.-C. Pei, "Design and application of discrete-time fractional Hilbert transformer," *IEEE Trans. Circuits Syst. II, Exp. Briefs*, vol. 47, no. 12, pp. 1529–1533, Dec. 2000.
- [13] R. Tao, X.-M. Li, and Y. Wang, "Generalization of the fractional Hilbert transform," *IEEE Signal Process. Lett.*, vol. 15, pp. 365–368, 2008.
- [14] T. Alieva, V. Lopez, F. Agullo-Lopez, and L. Almeida, "The fractional Fourier transform in optical propagation problems," *J. Modern Opt.*, vol. 41, no. 5, pp. 1037–1044, May 1994.

- [15] Y. Cai and F. Wang, "Lensless optical implementation of the coincidence fractional Fourier transform," *Opt. Lett.*, vol. 31, no. 15, pp. 2278–2280, Aug. 2006.
- [16] H. M. Ozaktas, D. Mendlovic, L. Onural, and B. Barshan, "Convolution, filtering, and multiplexing in fractional Fourier domains and their relation to chirp and wavelet transforms," *J. Opt. Soc. Amer. A, Opt. Image Sci.*, vol. 11, no. 2, pp. 547–559, Feb. 1994.
- [17] M. Kutay and H. M. Ozaktas, "Optimal image restoration with the fractional Fourier transform," *Comput. Standards Inter.*, vol. 20, nos. 6–7, pp. 452–453, Mar. 1999.
- [18] D. Mendlovic, H. M. Ozaktas, and A. W. Lohmann, "Fractional correlation," *Appl. Opt.*, vol. 34, no. 2, pp. 303–309, Jan. 1995.
- [19] D. Mendlovic, R. G. Dorsch, A. W. Lohmann, and Y. Bitran, "Optical fractional correlation: Experimental results," *J. Opt. Soc. Amer. A, Opt. Image Sci.*, vol. 12, no. 8, p. 1665, Aug. 1995.
- [20] T. Setälä, T. Shirai, and A. T. Friberg, "Fractional Fourier transform in temporal ghost imaging with classical light," *Phys. Rev. A, Gen. Phys.*, vol. 82, no. 4, 2010, Art. no. 043813.
- [21] D. Lu, W. Hu, Y. Zheng, Y. Liang, L. Cao, S. Lan, and Q. Guo, "Self-induced fractional Fourier transform and revivable higher-order spatial solitons in strongly nonlocal nonlinear media," *Phys. Rev. A, Gen. Phys.*, vol. 78, no. 4, 2008, Art. no. 043815.
- [22] V. Namias, "The fractional order Fourier transform and its application to quantum mechanics," *IMA J. Appl. Math.*, vol. 25, no. 3, pp. 241–265, 1980.
- [23] S. Granieri, O. Trabocchi, and E. Sicre, "Fractional Fourier transform applied to spatial filtering in the Fresnel domain," *Opt. Commun.*, vol. 119, nos. 3–4, pp. 275–278, Sep. 1995.
- [24] L. F. López-ávila, "Bidimensional correlation to recognize objects using the fractional Fourier transform," M.S. thesis, Dept. App. Phys., CICESE, Ensenada, Mexico, 2017.
- [25] E. Garza-Flores and J. Álvarez-Borrego, "Pattern recognition using binary masks based on the fractional Fourier transform," *J. Mod. Opt.*, vol. 65, no. 14, pp. 1634–1657, Aug. 2018.
- [26] R. Bracewell, *Fourier Analysis and Imaging*, 3rd ed. New York, NY, USA: Springer, 2000.
- [27] J.-B. Martens, "The Hermite transform-theory," *IEEE Trans. Acoust., Speech, Signal Process.*, vol. 38, no. 9, pp. 1595–1606, Sep. 1990.
- [28] B. Escalante-Ramírez and A. López-Caloca, "Image fusion with the Hermite transform," in *Proc. Int. Conf. Image Process. (ICIP)*, vol. 2, Sep. 2003, p. II-145.
- [29] A. Estudillo-Romero and B. Escalante-Ramírez, "The Hermite transform: An alternative image representation model for Iris recognition," in *Proc. Iberoamerican Congr. Pattern Recognit.* Berlin, Germany: Springer, 2008, pp. 86–93.
- [30] L. Barba-J, E. Moya-Albor, B. Escalante-Ramírez, J. Brieva, and E. V. Venegas, "Segmentation and optical flow estimation in cardiac CT sequences based on a spatiotemporal PDM with a correction scheme and the Hermite transform," *Comput. Biol. Med.*, vol. 69, pp. 189–202, Feb. 2016.
- [31] L. Vargas-Quintero, B. Escalante-Ramírez, L. C. Marín, M. G. Huerta, F. A. Cosio, and H. B. Olivares, "Left ventricle segmentation in fetal echocardiography using a multi-texture active appearance model based on the steered Hermite transform," *Comput. Methods Programs Biomed.*, vol. 137, pp. 231–245, Dec. 2016.
- [32] B. Escalante-Ramírez and A. A. López-Caloca, "The Hermite transform: An efficient tool for noise reduction and image fusion in remote-sensing," *Image Process. Remote Sens.*, vol. 273, pp. 537–555, Oct. 2007.
- [33] B. Escalante-Ramírez, "The Hermite transform as an efficient model for local image analysis: An application to medical image fusion," *Comput. Electr. Eng.*, vol. 34, no. 2, pp. 99–110, Mar. 2008.
- [34] M. Mackenzie and A. Tieu, "Hermite neural network correlation and application," *IEEE Trans. Signal Process.*, vol. 51, no. 12, pp. 3210–3219, Dec. 2003.
- [35] O. Akay and G. Boudreaux-Bartels, "Fractional convolution and correlation via operator methods and an application to detection of linear FM signals," *IEEE Trans. Signal Process.*, vol. 49, no. 5, pp. 979–993, May 2001.
- [36] D. Mustard, "Fractional convolution," *ANZIAM J.*, vol. 40, no. 2, pp. 257–265, 1998.
- [37] L. P. Yaroslavsky, "III the theory of optimal methods for localization of objects in pictures," *Progr. Opt.*, vol. 32, pp. 145–201, 1993.
- [38] B. V. K. V. Kumar and L. Hassebrook, "Performance measures for correlation filters," *Appl. Opt.*, vol. 29, no. 20, p. 2997, Jul. 1990.
- [39] A. Castro-Valdez and J. Álvarez-Borrego, "Identification of phytoplankton species using Hermite transform," *Ukrainian J. Phys. Opt.*, vol. 19, no. 2, pp. 106–120, 2018.



ALFREDO CASTRO-VALDEZ was born in Ensenada, Baja California, Mexico, in 1991. He received the B.S. degree in physics from UABC, in 2015, and the M.Sc. degree from CICESE, Baja California, in 2017, where he is currently pursuing the Ph.D. degree. His research interests include image processing and pattern recognition.



JOSUÉ ÁLVAREZ-BORREGO received the B.S. degree in physical oceanography from the Facultad de Ciencias Marinas, Ensenada, Baja California, Mexico, in 1981, and the M.Sc. and Ph.D. degrees in optics from CICESE, Mexico, in 1983 and 1993, respectively. He is currently a Professor with the Applied Physics Division, Optics Department, CICESE. His research interests are image processing with applications to biogenic particles and image processing of the sea surface. He is also the President of the Mexican Academy of Optics. He is also a member of the National Research System (SNI) and the Mexican Sciences Academy.

• • •